Assessing the risk to develop a growing teratoma syndrome based on molecular and epigenetic subtyping as well as novel secreted biomarkers

Pailin Pongratanakul, Felix Bremmer, Stella Pauls, Gereon Poschmann, Catena Kresbach, Fatma Parmaksiz, Margaretha A. Skowron, Janina Fuß, Alexa Stephan, Pia Paffenholz, Kai Stühler, Ulrich Schüller, Philipp Ströbel, Axel Heidenreich, Yue Che, Peter Albers, Daniel Nettersheim

Article - Version of Record

Suggested Citation:
Pongratanakul, P., Bremmer, F., Pauls, S., Poschmann, G., Kresbach, C., Parmaksiz, F., Skowron, M. A., Fuß, J., Stephan, A., Paffenholz, P., Stühler, K., Schüller, U., Ströbel, P., Heidenreich, A., Che, Y., Albers, P., & Nettersheim, D. (2024). Assessing the risk to develop a growing teratoma syndrome based on molecular and epigenetic subtyping as well as novel secreted biomarkers. Cancer Letters, 585, Article 216673. https://doi.org/10.1016/j.canlet.2024.216673

Cancer Letters 585 (2024) 216673

Contents lists available at ScienceDirect

Cancer Letters

journal homepage: www.elsevier.com/locate/canlet

Original Articles

Assessing the risk to develop a growing teratoma syndrome based on molecular and epigenetic subtyping as well as novel secreted biomarkers

Pailin Pongratanakul [a,g,1], Felix Bremmer [b,1], Stella Pauls [c], Gereon Poschmann [c], Catena Kresbach [d], Fatma Parmaksiz [a], Margaretha A. Skowron [a], Janina Fuß [e], Alexa Stephan [a], Pia Paffenholz [f], Kai Stühler [c], Ulrich Schüller [d], Philipp Ströbel [b], Axel Heidenreich [f], Yue Che [g], Peter Albers [g], Daniel Nettersheim [a,h,*]

[a] Department of Urology, Urological Research Laboratory, Translational UroOncology, Medical Faculty and University Hospital Düsseldorf, Heinrich Heine University Düsseldorf, Düsseldorf, Germany
[b] Institute of Pathology, University Medical Center Goettingen, Goettingen, Germany
[c] Molecular Proteomics Laboratory (MPL), Biological and Medical Research Center (BMFZ), Medical Faculty and University Hospital Düsseldorf, Heinrich Heine University Düsseldorf, Düsseldorf, Germany
[d] Institute of Neuropathology, University Hospital Hamburg-Eppendorf, Hamburg, Germany
[e] Competence Centre for Genomic Analysis, Kiel, Germany
[f] Department of Urology, University Hospital Cologne, University of Cologne, Cologne, Germany
[g] Department of Urology, Medical Faculty and University Hospital Düsseldorf, Heinrich Heine University Düsseldorf, Düsseldorf, Germany
[h] Lighthouse Project Germ Cell Tumors, Center for Integrated Oncology Aachen Bonn Cologne Duesseldorf (CIO ABCD), Germany

ARTICLE INFO

Keywords:
Germ cell tumors
Growing teratoma syndrome
Teratoma
DNA methylation
Secretome
Proteome
Biomarker

ABSTRACT

In germ cell tumors (GCT), a growing teratoma during chemotherapy with decreasing tumor markers was defined as 'growing teratoma syndrome' (GTS) by Logothetis et al. in 1982. So far, its pathogenesis and specific treatment options remain elusive.

We aimed at updating the GTS definition based on molecular and epigenetic features as well as identifying circulating biomarkers. We selected 50 GTS patients for clinical characterization and subsequently 12 samples were molecularly analyzed. We further included 7 longitudinal samples of 2 GTS patients. Teratomas (TER) showing no features of GTS served as controls.

GTS were stratified based on growth rates into a slow (<0.5 cm/month), medium (0.5–1.5) and rapid (>1.5) group. By analyzing DNA methylation, microRNA expression and the secretome, we identified putative epigenetic and secreted biomarkers for the GTS subgroups. We found that proteins enriched in the GTS groups compared to TER were involved in proliferation, DNA replication and the cell cycle, while proteins interacting with the immune system were depleted. Additionally, GTS^{rapid} seem to interact more strongly with the surrounding microenvironment than GTS^{slow}. Expression of pluripotency- and yolk-sac tumor-associated genes in GTS and formation of a yolk-sac tumor or somatic-type malignancy in the longitudinal GTS samples, pointed at an additional occult non-seminomatous component after chemotherapy. Thus, updating the Logothetis GTS definition is necessary, which we propose as follows:

The GTS describes a continuously growing teratoma that might harbor occult non-seminomatous components considerably reduced during therapy but outgrowing over time again.

1. Introduction

Testicular germ cell tumors (GCT) are the most common malignancy among young men, appearing in different or mixed histological entities classified into seminomas and non-seminomas [1]. The latter has its own stem-cell-like population, the embryonal carcinoma (EC), which is able

* Corresponding author. Department of Urology, Urological Research Laboratory, Translational UroOncology, Medical Faculty and University Hospital Düsseldorf, Heinrich Heine University, Moorenstraße 5, 40225, Düsseldorf, Germany.
E-mail address: Daniel.Nettersheim@med.uni-duesseldorf.de (D. Nettersheim).
[1] Contributed equally.

https://doi.org/10.1016/j.canlet.2024.216673
Received 30 October 2023; Received in revised form 17 January 2024; Accepted 21 January 2024
Available online 29 January 2024

to differentiate into all three germ layers (teratoma (TER)), and into extra-embryonic tissue, i. e. yolk-sac tumors (YST) and choriocarcinomas (CC) [1].

During cisplatin-based standard chemotherapy, some patients present with a growing tumor mass on imaging, while serum tumor markers (alpha-fetoprotein (AFP), beta-human choriogonadotropin (beta-hCG), lactate dehydrogenase (LDH)) decreased or normalized. In these cases, complete surgical resection represents the only treatment option, revealing pure mature teratoma without evidence of other GCT entities in the final pathology. This phenomenon was first described by Logothetis et al. in 1982 based on six case reports and is called the 'growing teratoma syndrome' (GTS) [2]. To date, only few studies analyzing the GTS have been published [3–6]. Due to the small number of available cases worldwide, not much is known about GTS and its pathogenesis. Especially in cases with very space-demanding and surgical uncontrollable tumor mass, specific therapies and biomarkers early indicating presence of GTS are still lacking.

We aimed at updating and extending the current understanding of GTS, which was established 42 years ago. This is the first study subtyping GTS based on the growth rate over time and characterizing these subgroups on epigenetic (DNA methylation and microRNA), transcriptional (mRNA) and proteome/secretome level. By this, we not only identified the molecular and epigenetic features of the GTS subtypes, but also identified risk factors for rapidly growing GTS. Additionally, we deduced novel circulating biomarkers for the GTS subtypes.

2. Material and methods

2.1. GTS patient cohort

We retrospectively reviewed data of GCT patients undergoing a post-chemotherapy retroperitoneal lymph node dissection (RPLND) at the Departments of Urology of the University Hospitals Düsseldorf (UKD) and Cologne (UKK) from 2010 to 2023. Based on the definition by Logothetis et al., we identified 39 (UKD) and 11 (UKK) patients with a growing, histologically pure TER during or after chemotherapy associated with a decrease or normalization of serum tumor markers (AFP, beta-hCG, LDH). For the calculation of the tumor growth rate (cm/month), the transversal tumor diameter before and after chemotherapy on computed tomography (CT) were measured. The increase of tumor size (cm) was then divided by the time (month, 30 days = 1 month) from the start of chemotherapy to RPLND.

2.2. GCT tissues and cell lines

GTS tissues (formalin-fixed, paraffin-embedded (FFPE) and fresh frozen) were collected from the local biobank of the Department of Urology at the UKD (stored at the Institute of Pathology). All tissues were re-evaluated by a reference pathologist for type II GCT (F. B.). The utilized GCT cell lines were provided and cultivated as described in Table S1 A.

2.3. Immunohistochemistry

Immunohistochemistry has been performed as described [7]. Antigen retrieval was performed in citrate buffer. The Ki67 antibody (ready-to-use, Agilent Dako, Waldbronn, Germany) was incubated for 30 min at room temperature (RT). Samples were incubated with a ready-to-use-HRP-labelled secondary antibody at RT for 25 min. The substrate 'DAB + Chromogen System' (Agilent Technologies, Waldbronn, Germany) was used to visualize the antigen. Tissues were counterstained with Meyer's hematoxylin.

2.4. Nucleic acid isolation

According to manufacturer's recommendations, DNA was extracted from 2×5 μm FFPE slides using the 'InnuPREP FFPE DNA Kit' on the 'InnuPure C16 System' (Jena Analytika, Jena, Germany). RNA was isolated by the TRIzol reagent according to the manual (Qiagen, Hilden, Germany). Nucleic acid concentrations and purities were measured by the 'Nanodrop 2000' photo-spectrometer (260/280 nm; 260/230 nm).

2.5. DNA methylation profiling

DNA methylation profiling was performed as described previously [8]. Briefly, 100–500 ng DNA were used for bisulfite conversion with the 'EZ DNA Methylation Kit' (Zymo Research, Freiburg. i. B., Germany). Afterwards, the 'DNA Clean & Concentrator-5' (Zymo Research) and the 'Infinium HD FFPE DNA Restore Kit' (Illumina, San Diego, CA, USA) were used to clean and restore the converted DNA. Finally, the 'Infinium 850k MethylationEPIC BeadChip' (850k array; Illumina) was used to evaluate the methylation status of 850,000 CpG sites on an 'iScan' device (Illumina).

2.6. Quantitative RT-PCR

cDNA synthesis and quantitative RT-PCR were performed as published previously [9]. 1 μg of total RNA was used for cDNA synthesis. Gene expression levels were determined on the 'C1000 cycler' (BioRad, Feldkirchen, Germany) using 7.34 ng cDNA and in technical triplicates. *GAPDH* and *ACTB* were used as housekeeping genes and for data normalization. For oligonucleotide details, see Table S1 B.

2.7. microRNA sequencing

Library preparation was done with the 'NEXTFLEX Small RNA-Seq Kit v4' (Revvity, Hamburg, Germany) according to manufacturer's protocol with 200 ng input. MicroRNA sequencing (microRNAseq) of the library pool was done on a full 'NovaSeq6000 SP' flow cell with a 'NovaSeq 6000 SP Reagent Kit v1.5 (100 cycles)'. Paired-end sequencing has been performed twice for each sample. Demultiplexing was done with bcl2fastq v2.20.0.422. Analysis was performed using 'nf-core/smrnaseq v2.2.0', against the human reference genome GRCh38. The statistical QC was performed using the 'FastQC' tool (https://www.bioinformatics.babraham.ac.uk/projects/fastqc/), generating the mean quality scores of all sequences, sequence duplication levels and the count of unique/duplicate reads. Counts per million were calculated by the TMM normalization method in the 'edge' R package [10,11]. The variance between samples was assessed using the f-test and the significance (p-value <0.05) was checked by two-tailed Student's t-tests.

2.8. Proteome and secretome analysis

2.8.1. Preparation of FFPE tissues for analysis

A modified FFPE tissue lysis protocol of Ikeda et al. was applied [12]. FFPE tissue slides were transferred with a scalpel into 1 mL protein-low binding tubes and deparaffinized by shaking in 500 μL xylene for 5 min, followed by removal of the solvent and air-drying. Next, tissues were resuspended in 200 μL lysis buffer (300 mM TRIS/HCl, 2 % SDS, pH 8.0), shock-frozen in liquid nitrogen and immediately heated for 25 min at 99 °C. For complete lysis, samples were ultrasonicated on ice for 20 min with 30 s on/off cycles and then shook or 2 h at 80 °C and 500 rpm, followed by a second ultrasonication step. After centrifugation, the supernatant was transferred into a new 0.5 mL protein-low binding tube and the pellet was resuspended in 100 μL buffer for a second extraction. The resulting supernatants were combined. Protein concentration was determined using the 'Pierce 660 nm Protein Assay' (Thermo Fisher Scientific, Bremen, Germany).

For liquid chromatography coupled to mass spectrometry (LC-MS) analysis, a modified magnetic bead-based sample preparation protocol was applied [13]. Briefly, 20 μg of total protein per sample was reduced by 10 μL 300 mM dithiothreitol (DTT) and shaking for 20 min at 56 °C

and 1000 rpm, followed by alkylation by 13 μL 100 mM IAA and incubation for 15 min in the dark. A 20 μg/μL bead stock of 1:1 'Sera-Mag SpeedBeads' was freshly prepared and 10 μL were added to each sample. Afterwards, ethanol was added to a final concentration of 80 % for protein aggregation and the sample was incubated for 15 min at 20 °C. After three washing steps with 80 % ethanol and one washing step with 100 % ACN, beads were resuspended in 50 mM TEAB buffer and digested with final 0.4 μg trypsin (1:50) at 37 °C and 1000 rpm overnight. Extra-digestion was carried out by adding trypsin (final 1:50) and shaking at 37 °C and 1000 rpm for 4 h. The supernatants were collected and 500 ng of each sample digest were diluted with 0.1 % TFA and subjected to LC-MS.

2.8.2. Secretome production and preparation for LC-MS analysis

0.5×0.2 cm slices of fresh frozen tissues were used for secretome production. For the removal of blood components, tumor slices were washed five times with 30 mL PBS. To avoid detecting secreted factors from a stress response, we carried out an initial incubation step in 400 μL serum-free medium at 37 °C and 7.5 % CO_2 on a 24-well plate and discarded the medium after 2 h. Before incubation in new 400 μL serum-free medium for 24 h, additional washing steps with 400 μL PBS (5x) were performed. The secretomes were collected and centrifuged twice at 1000 g for 5 min and 3000 g for 10 min at 4 °C. According to manufacturer's recommendation (Roche, Mannheim, Germany), a protease inhibitor cocktail was prepared and 50 μL were added to the secretome. For protein precipitation, trichloroacetic was added. Protein concentrations were determined by the 'Pierce 660 nm Protein Assay' (Thermo Fisher Scientific). Five μg of each supernatant was prepared by in-gel digestion as described previously [14]. Briefly, samples were loaded and separated on a polyacrylamide gel. After staining with Coomassie Brilliant blue, proteins were reduced with DTT, alkylated with iodoacetamide and digested with trypsin. Tryptic peptides (about 500 ng/sample) were prepared for LC-MS analysis in an aqueous solution of 0.1 % trifluoroacetic acid.

2.8.3. LC-MS analysis

For LC-MS, an 'Orbitrap Fusion Lumos Tribrid Mass Spectrometer with FAIMS' (Thermo Fisher Scientific) coupled to an 'Ultimate 3000 Rapid Separation' liquid chromatography system (Thermo Fisher Scientific, Idstein, Germany) equipped with an 'Acclaim PepMap 100C18 column' (75 μm inner diameter, 25 cm length, 2 mm particle size from Thermo Fisher Scientific) as separation column and an 'Acclaim PepMap 100C18 column' (75 μm inner diameter, 2 cm length, 3 mm particle size; Thermo Fisher Scientific) as trap column were used. A LC-gradient of 120 min separation duration was applied. The mass spectrometer was operated in positive data independent acquisition mode, the capillary temperature was set to 275 °C, the source voltage to 2.0 kV. It was additionally equipped with a FAIMS device (carrier gas flow: 4.5 L/min., compensation voltage (CV): 50 V). Precursor spectra were recorded in the orbitrap analyzer within a scan range of 380–985 m/z at a resolution of 60,000 (automatic gain control target value: 400,000, maximum injection time: 100 ms). Precursors were selected within isolation windows of 10 m/z (with an overlap of 1 m/z) within a precursor mass range of 380–980 m/z. After fragmentation by higher energy collisional dissociation (30 % collision energy, 5 % stepped collision energy), fragment spectra (scan range 145–1450 m/z) were recorded in the orbitrap analyzer at a resolution of 15,000 (automatic gain control target value: 100,000, maximum injection time: 40 ms). Cycle time was set to 3 s.

2.8.4. LC-MS raw data processing

Data analysis was carried out with 'DIA-NN' (version 1.8.1, https://github.com/vdemichev/DiaNN) [15]. All raw files were searched against the human proteome 'UniProt KB' dataset (UP000005640, downloaded on 12.01.2023) and the 'Maxquant Contaminant' database (downloaded on 03.05.2022), using the deep learning tool to generate an *in silico* spectral library, which is implemented in 'DIA-NN'. The digestion enzyme was set to trypsin, the maximum number of missed cleavages was set to two (one for tissue secretome) and the peptide length was 7–30 amino acids. Mass accuracy was optimized by 'DIA-NN' using the first run in the experiment. As variable modifications were methionine oxidation, N-terminal methionine loss and methylation of lysines (only for FFPE tissues) defined. Fixed modification was carbamidomethylation of cysteines. All samples were analyzed in a match between run (MBR) search. During post processing, peptides were ungrouped and filtered to 1 % FDR on protein and peptide level and to all proteins identified with ≥2 peptides. Contaminants were filtered out and the results were exported as excel sheet.

2.8.5. LC-MS data analysis of FFPE tissues

All samples were normalized by comparing each 'MaxLFQ' value of a protein to the corresponding value of a selected reference sample and the medians of the resulting $\log_2$ fold changes (FC) were set to zero. The sample with the highest number of positive medians (of $\log_2$ FC) was selected as reference. All other samples were normalized by multiplying the 'MaxLFQ' intensities with the calculated, delogarithmized medians of $\log_2$ FC. All samples, except the samples of the longitudinal comparison undergo imputation of missing values from random numbers drawn from a defined width (0.3) and downshift (1.8) of the Gaussian distribution relative to the standard deviation of measured values. Protein abundance of different sample groups was compared by SAM analysis [16], carried out using R (version 4.2.3) with the 'sam()' function of the 'siggenes' package (version 1.72.0). Gene ontology clustering of samples that undergo longitudinal proteomic analysis were carried out using the 'Mfuzz' package (version 2.58.0) for R.

2.8.6. LC-MS data analysis of secretomes

Analysis of quantitative proteome data was carried out with 'Perseus 1.6.6.0' (Max-Planck Institute for Biochemistry, Planegg, Germany). Only proteins showing at least three valid values in at least one sample group were considered for further analysis (and statistical testing). Missing values of $\log_2$ transformed normalized intensities (MaxLFQ) were filled in with values drawn from a downshifted normal distribution (width 0.3, downshift 1.8 standard deviations). Differences between groups were determined by ANOVA as well as 'significance analysis of microarrays' $(SAM)^4$ using an S^0 of 0.1 and permutation based false discovery rate set to 5 %. The secretion behavior or protein was predicted by 'OutCyte' [17].

2.8.7. Online analysis tools

Online analysis tools like 'STRING' (https://string-db.org/) and the 'DAVID Functional Annotation Tool' using 'GOTERM_BP_DIRECT', 'GOTERM_MF_DIRECT' and 'KEGG_PATHWAY' (https://david.ncifcrf.gov) were used to predict protein interactions and their molecular functions. LC-MS data were evaluated by a principle component analysis using 'PCAGO' (https://pcago.bioinf.uni-jena.de/). The 'pandas', 'seaborn', and 'matplotlib' libraries were used in 'Python' for generation of Pearson's correlation matrices and volcano plots. The 'The Cancer Genome Atlas' (TCGA) GCT cohort was analyzed using 'cBioPortal' (https://www.cbioportal.org/) [18,19].

3. Results

In this study, we identified 50 GTS patients (Table 1). 43 patients presented with metastatic disease at first diagnosis, while 7 patients presented metastases during surveillance with clinical stage II and III in 33 and 17 cases, respectively. Prognosis based on the International Germ Cell Cancer Collaborative Group (IGCCCG) classification was mostly favorable, with good, intermediate and poor prognosis in 34, 7 and 9 cases, respectively. Initially, serum tumor markers AFP and beta-hCG were elevated (>7 μg/l) in 44 and 39 patients, respectively. Every patient received platin-based chemotherapy with a majority of 90 %

Table 1
Clinical parameters of GTS patients treated at the Dept. of Urology of the University Hospital Düsseldorf and University Hospital Cologne included in this study.

GTS patient and tumor characteristics				
Tumor growth classification	all	slow	medium	rapid
Number	50 (46*)	19	21	6
Median age at diagnosis	27 (16 - 47)	31 (21 - 44)	26 (16 - 47)	28 (22 - 34)
Clinical stage				
II	33 (66 %)	15 (79 %)	14 (67 %)	4 (67 %)
III	17 (34 %)	4 (21 %)	7 (33 %)	2 (33 %)
IGCCCG classification				
good risk	34 (68 %)	16 (84 %)	14 (67 %)	4 (67 %)
intermediate risk	7 (14 %)	0 (0 %)	6 (28 %)	0 (0 %)
poor risk	9 (18 %)	3 (16 %)	1 (5 %)	2 (33 %)
Tumor marker initial*				
AFP >7.0 µg/l	44 (88 %)	18 (95 %)	17 (81 %)	6 (100 %)
β-HCG >2.0 mU/ml	39 (78 %)	14 (74 %)	17 (81 %)	4 (67 %)
both elevated	36 (72 %)	14 (74 %)	15 (71 %)	4 (67 %)
Tumor marker after chemotherapy				
negative	42 (84 %)	17 (89 %)	17 (81 %)	4 (67 %)
decreased	8 (16 %)	2 (11 %)	4 (19 %)	2 (33 %)
Initial clinical stage				
primary metastastic	43 (86 %)	16 (84 %)	18 (86 %)	5 (83 %)
metastatic recurrence	7 (14 %)	3 (16 %)	3 (14 %)	1 (17 %)
Tumor localization				
retroperitoneum	50 (100 %)	19 (100 %)	21 (100 %)	6 (100 %)
pulmonary	3 (6 %)	1 (5 %)	2 (10 %)	0 (0 %)
retrocrural	7 (14 %)	2 (11 %)	3 (14 %)	1 (17 %)
liver	3 (6 %)	1 (5 %)	1 (5 %)	0 (0 %)
clavicular	2 (4 %)	1 (5 %)	1 (5 %)	0 (0 %)
Primary tumor histology				
pure teratoma	5 (10 %)	2 (11 %)	3 (14 %)	0 (0 %)
mix with teratoma	34 (68 %)	10 (53 %)	16 (76 %)	5 (83 %)
mix with embryonal carcinoma	39 (78 %)	14 (74 %)	16 (76 %)	5 (83 %)
mix with yolk-sac tumor	20 (40 %)	3 (16 %)	11 (52 %)	4 (67 %)
mix with choriocarcinoma	9 (18 %)	4 (21 %)	3 (14 %)	0 (0 %)
Chemotherapy				
3–4 x PEB	45 (90 %)	17 (89 %)	19 (90 %)	6 (100 %)
4 x PE/PEI	4 (8 %)	2 (11 %)	1 (5 %)	0
3 x TIP	1 (2 %)	0 (0 %)	1 (5 %)	0

* Median tumor marker levels [interquartile range]	AFP (µg/l)	β-HCG (mU/ml)
all	181.5 [15.8–221129]	164 [2.7–31844]
slow	147.5 [15.8–22129]	90 [6–11936]
medium	153 [18–9937]	139.5 [6.2–5827]
rapid	270 [27 - 40282]	6322 [66.5–31844]

receiving 3–4 cycles of the regime cisplatin, etoposide and bleomycin (BEP). After chemotherapy, serum tumor markers were normalized in 42 and decreased to low but still slightly elevated (7.9–43 µg/l) levels in 8 patients. In terms of tumor manifestation, GTS formation was always found retroperitoneal (n = 50). Other additional localizations were retrocrural (n = 7), lung (n = 3), liver (n = 3), and clavicular or cervical lymph nodes (n = 2).

Measurements of the transversal tumor diameter of the retroperitoneal mass before and after chemotherapy on CT scans for the calculation of the tumor growth rate were available for 46 of 50 GTS patients. Based on the tumor growth rate, patients were arbitrarily stratified into a slow (<0.5 cm/month), medium (0.5–1.5) and rapid (>1.5) group (Fig. 1 A). The median tumor growth rate was 0.8 cm/month (0.06–3.6 cm/month) (Fig. 1 B). Exemplary CT scans of the GTS subgroups before and after chemotherapy are shown in Fig. 1 C.

Next, we characterized each GTS subgroup based on molecular and epigenetic features to identify putative biomarkers on epigenetic (DNA methylation and microRNA) and protein level (Fig. 2 A). We included three samples each of slow, medium and rapid GTS as well as three samples of TER without a growth trend as controls (Fig. 1 A, asterisks).

Histomorphologically, the GTS subgroups showed typical TER features with cells of all three germ layers, resulting in detection of tissue structures like cartilage, smooth muscle or endothelium (Fig. S1 A - C). We stained all GTS groups for Ki67 to identify proliferating cell populations that might fuel GTS growth (Fig. S1 D). We detected mainly $Ki67^+$ endothelial cells and single $Ki67^+$ cells within the tumor or at its borders, but without significant differences between the GTS subgroups (Fig. S1 D). Thus, the distribution of Ki67+ cells in the GTS subgroups does not explain the differences in growth rates or tumor volume.

By using 850k DNA methylation arrays, we analyzed the DNA methylation (5mC) landscape of TER and GTS samples (Data S1 A). Genome-wide, all analyzed samples showed a highly comparable distribution of DNA methylation (Fig. 2 B, inlay). Regarding site-specific DNA methylation, we identified hypo- (<20 % 5mC) and hypermethylated (>80 % 5mC) CpG dinucleotides for each GTS group and analyzed their distribution across the genome (in gene coding and CpG island context) (Fig. S2 A; Data S1 B). In all groups, hypermethylated CpG dinucleotides were mainly found within gene bodies and open sea context, while hypomethylated CpG dinucleotides were mainly found in transcription start sites (TSS; TSS200, TSS1500) and CpG island context (Fig. S2 A). By Venn diagrams, we compared all hypo- and hypermethylated CpG dinucleotides found in the different groups to each other and identified commonly shared and individual CpG dinucleotides (Fig. S2 B). To identify putative epigenetic biomarkers, we identified CpG dinucleotides exclusively hypermethylated (>10-fold change in 5mC) in the different subgroups (GTS^{slow} vs. TER, GTS^{rapid} vs. TER, GTS^{rapid} vs. GTS^{slow}, $GTS^{slow/rapid}$ vs. TER) (Fig. 2 B, Data S1 B).

To identify further epigenetic biomarkers, we performed microRNAseq and demonstrated that the global microRNA expression profile of GTS^{slow} and GTS^{rapid} was more similar to each other than to TER (Fig. 2 C, inlay). We identified microRNAs able to distinguish GTS^{slow} from TER [13], GTS^{rapid} from TER [8], and GTS^{rapid} from GTS^{slow} [12] (FC >2; p-value <0.05) (Fig. 2 C; Data S1 C).

Additionally, by LC-MS, we analyzed the secretomes of GTS and TER samples to identify secreted biomarkers (Data S1 D). A heatmap including unsupervised hierarchical clustering demonstrated that on secretome level, the GTS^{slow} were more similar to TER than to GTS^{rapid} (Fig. 2 D, inlay). We screened for putative secreted biomarkers (signaling peptides and unconventional protein secretion (UPS)) indicative for the different GTS subgroups versus TER (with a FC >2) (Data S1 E). We identified 19 proteins specifically detected in GTS^{slow} vs. TER, 53 in GTS^{rapid} vs. TER, and 10 proteins in $GTS^{slow/rapid}$ vs. TER, which might serve as individual biomarkers (Fig. 2 C). Additionally, we identified putative biomarkers able to discriminate GTS^{rapid} from GTS^{slow} (Fig. 2 D, inlay).

Of note, biomarkers specifically identifying TER are lacking. Thus, to identify general biomarkers for TER, we detected all secreted proteins (secreted peptides [31] and UPS (50)) with high intensity in all analyzed samples (TER+GTS; threshold 10×10^6) (Fig. S2 B). To confirm our findings, we screened the TCGA GCT cohort for the mRNA expression of the putative biomarkers, demonstrating that indeed most of these factors where highly expressed in TER and mixed GCT with TER component (Fig. S3, asterisks).

So far, our study highlighted putative biomarkers on DNA methylation, microRNA and secretome level.

Now, we further extended our molecular characterization of the GTS by performing LC-MS of FFPE tissue slides (Data S1 F). Proteomes of GTS and TER were compared by a principle component analysis (PCA). Here, all GTS samples clustered apart from TER (with exception of 1 sample) (Fig. 3 A). A Pearson's correlation matrix (PCM) showed a decreasing similarity of GTS to TER with increasing growth speed, i. e. GTS^{rapid} shows the least similarity to TER within the GTS groups (Fig. 3 B). To identify unique molecular features of GTS, we focused the analysis on the two subgroups GTS^{slow} and GTS^{rapid} as extremes within the spectrum

A

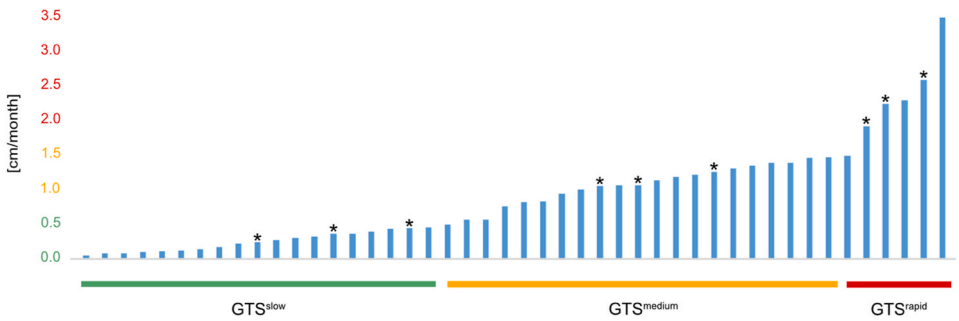

B

Tumor growth				
tumor growth classification	all (n = 46)	slow (n = 19)	medium (n = 21)	rapid (n = 6)
median tumor size initial [cm]	4.85 (0.9 - 30)	3.9 (0.9 - 13)	5.1 (1.1 - 30)	9.15 (5.7 - 14)
median tumor size after chemotherapy [cm]	8.7 (2 - 36)	5.3 (2 - 14)	9.0 (3 - 36)	16.8 (10.5 - 25)
median tumor growth rate [cm / month]	0.8 (0.06 - 3.6)	0.25 (0.06 - 0.46)	1.07 (0.51 - 1.48)	2.28 (1.5 - 3.6)

C

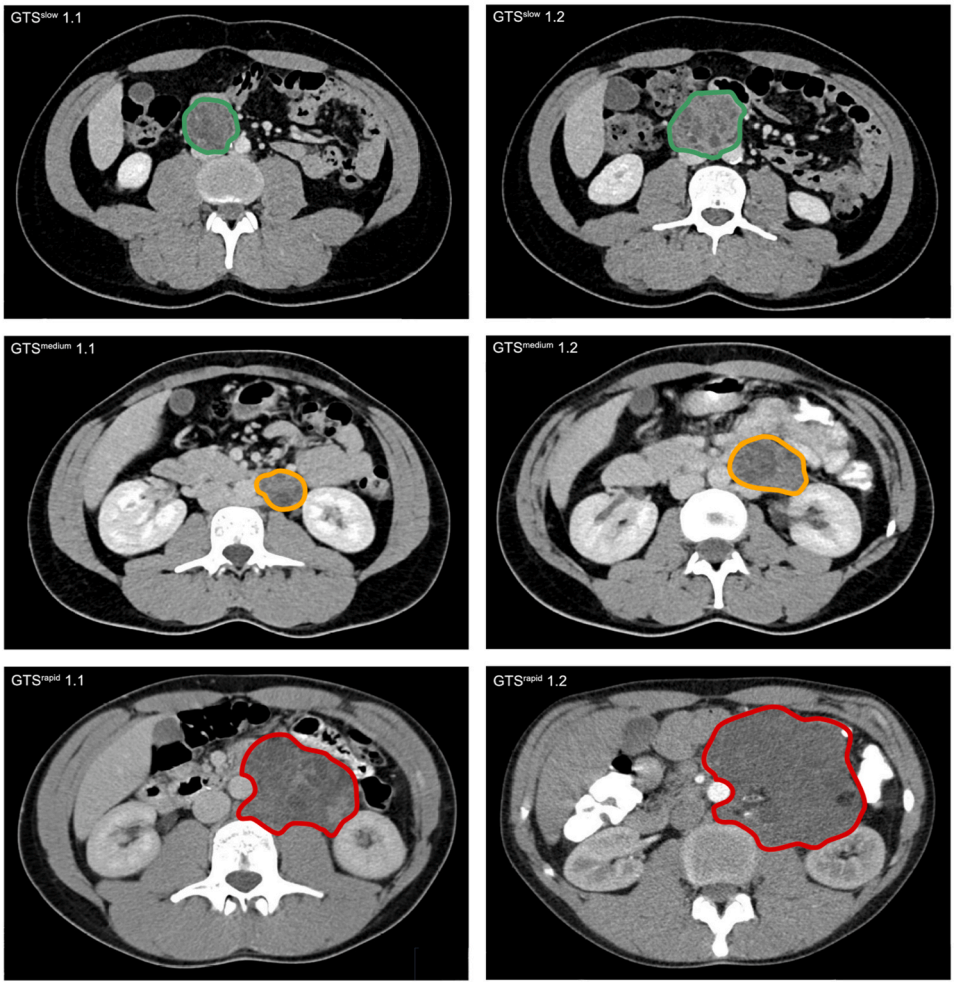

Fig. 1. A, B) Subtyping of GTS (slow, medium, rapid) based on the speed of growth (cm/month). C) Examples of slow (green), medium (orange) and rapid (red) GTS growth in CT scans before and after chemotherapy.

of GTS samples (Data S1 G). We compared their proteomes by using volcano plots, where 144 and 131 proteins were enriched compared to TER, respectively (Fig. 3 C). In contrast, 133 and 223 proteins were depleted compared to TER (Fig. 3 C). By using the STRING and DAVID algorithms, we screened for putative protein interactions and functional clustering (Fig. 3 D, E). Proteins found enriched in all GTS are involved in processes like DNA replication and unwinding, DNA repair, ATP-related processes and the cell cycle, while mainly proteins associated with an immune response and the immune system in general were depleted compared to TER (Fig. 3 D). Moreover, exclusively in GTS^{rapid}, further immune-related processes like the complement and coagulation cascade, the adaptive and humoral immune response, neutrophil extracellular trap formation, and the inflammatory or defense response were depleted. Additionally, apoptosis-associated processes were

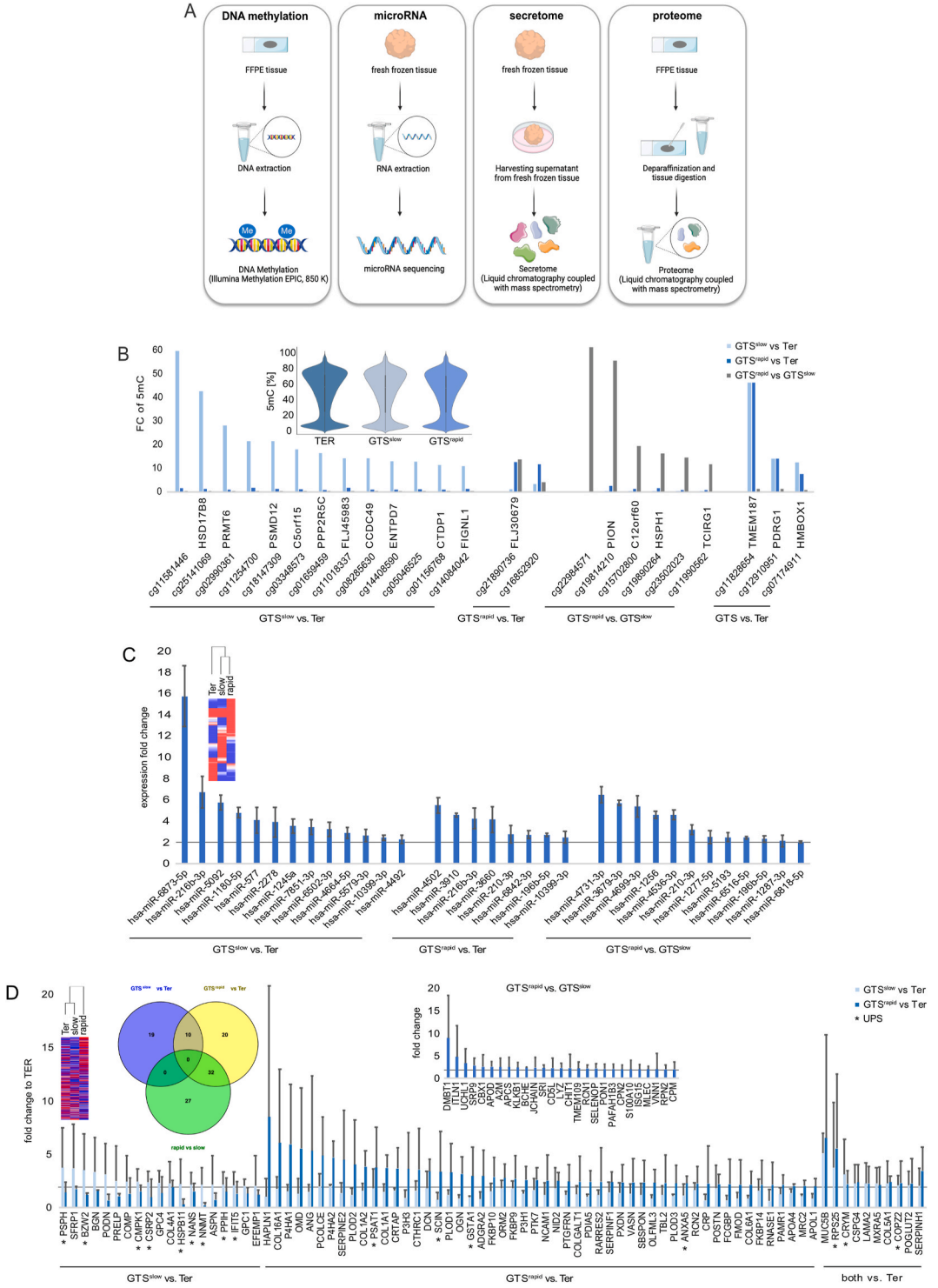

Fig. 2. A) Overview of the experiments performed in this study. B) Exclusively hypermethylated (>10-fold change in 5mC) CpG dinucleotides in the different GTS subgroups serving as possible biomarkers. Inlay: % distribution of global 5mC levels in GTS and TER samples. C) Differentially expressed microRNAs between the GTS groups and compared to TER (FC >2). Inlay: A heatmap including hierarchical clustering shows similarities between the microRNA expression profiles. D) Individually secreted biomarkers for the different GTS subgroups. Inlays left side: A heatmap including hierarchical clustering shows similarities between the secretomes. A Venn diagram demonstrates differences and similarities between the secretomes of the different GTS subgroups (compared to TER). Inlay in middle: Biomarkers indicative for GTS^{rapid} versus GTS^{slow}.

depleted (Fig. 3 D). The STRING algorithm predicted interaction of enriched and depleted proteins in each GTS group compared to TER (Fig. 3 E).

Of note, in the sets of enriched or depleted proteins found in GTS^{medium} samples, we detected similar corresponding functional terms as found in both, the GTS^{slow} and GTS^{rapid} samples (Fig. S4 A–C).

Finally, we asked how GTS develops in a patient over time. Therefore, we included longitudinal data of two GTS patients treated in our Department of Urology (UKD); with patient 1 and 2 representative for GTS^{slow} and GTS^{rapid} based on the initial growth dynamics of the GTS,

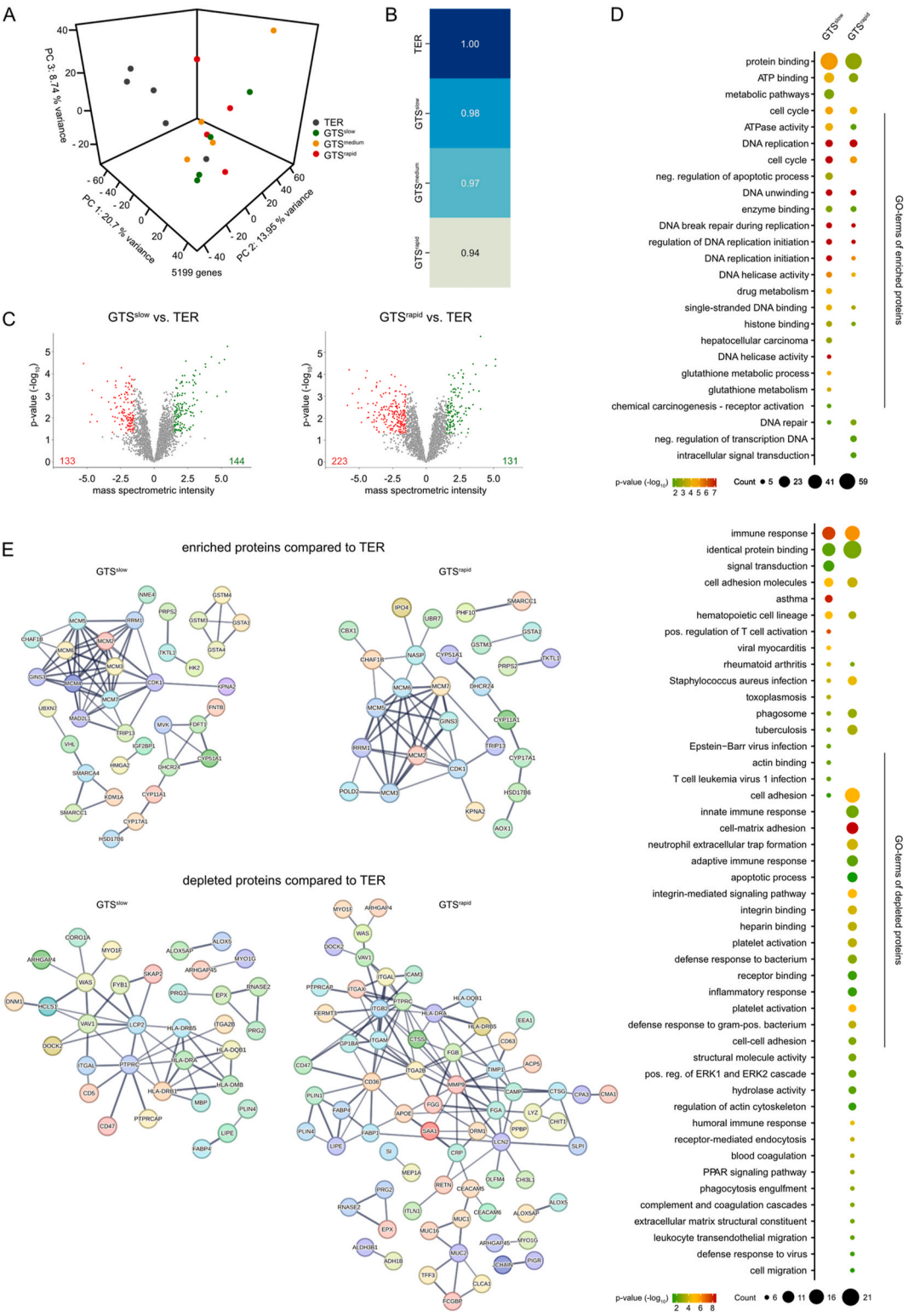

Fig. 3. A) A PCA of the proteome data from TER and the different GTS subgroups. B) A PCM compares the GTS subgroups to TER. C) Volcano plots illustrate proteins significantly enriched (green) or depleted (red) in GTS^{slow} and GTS^{rapid} compared to TER. D) Biological processes and functions of proteins found enriched in GTS compared to TER predicted by the DAVID algorithm. E) STRING-based protein-protein-interaction prediction of proteins found enriched/depleted in GTS^{slow} and GTS^{rapid} compared to TER.

respectively (Fig. 4 A). Both patients were diagnosed with a primary metastatic GTS. In patient 1, the initial tumor manifested mainly retroperitoneal, but was also found mediastinal and supraclavicular (Fig. 4 A). Over a time period of 13 years, patient 1 had developed 9 recurrences in the retroperitoneum only, starting with multiples TER, followed by YST and then a somatic-type malignancy (STM) (Fig. 4 A). During the relapse period, AFP was always elevated between 16.6 μg/l and 500 μg/l. Patient 2 had 8 recurrences in 8 years (Fig. 4 A). After receiving several systemic therapies due to persistent high AFP level, the tumor metastasized into the lung and brain, showing YST for the first

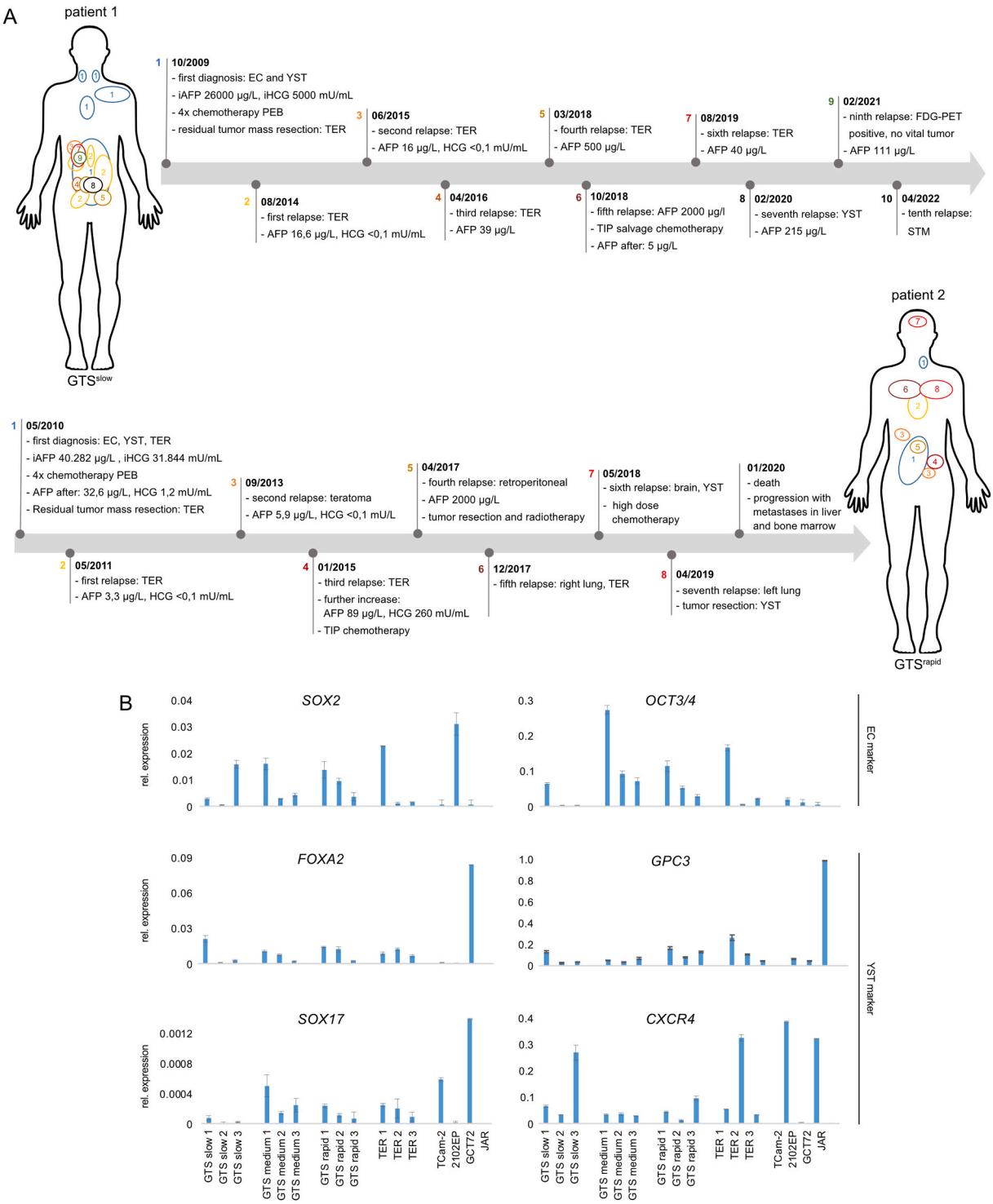

Fig. 4. A) Longitudinal clinical data of two GTS patients treated at the Department of Urology (UKD). Localization of each tumor/relapse is given in the pictogram of a human. B) qRT-PCR analysis of EC (*SOX2*, *OCT3/4*) and YST (*FOXA2*, *GPC3, SOX17, CXCR4*) marker genes in GTS and TER. GCT cell lines served as controls (TCam-2 = SEM; 2102EP = EC; GCT72 = YST; JAR = CC). *GAPDH* and *beta-ACTIN* served as housekeeping genes and were used for normalization.

time (Fig. 4 A). The tumor progressed rapidly with infiltration of the liver and bone marrow, subsequently, patient 2 died unfortunately. Taking both longitudinal cases into account, we observed teratomatous recurrences although AFP was elevated and steadily increasing over time, resulting in formation of YST (both patients) and even a STM (patient 1). These longitudinal data support the idea of a residual, but pathological not detectable (occult) subpopulation of EC or YST within the GTS. A hypothesis confirmed by us by qRT-PCR analysis of EC and YST markers in GTS tissues (Fig. 4 B). Moderate but detectable expression of *SOX2* and *OCT3/4* (EC markers) as well as *FOXA2, GPC3, SOX17* and *CXCR4* (YST markers) suggests that most of these GTS samples also harbor an occult EC and/or YST component (Fig. 4 B) [20–22].

To gain insight into the underlying molecular mechanisms driving the GTS progression longitudinally, FFPE slides of the initial tumor and selected relapses were analyzed by LC-MS and compared by a PCA and PCM (Fig. 5 A, B). In both patients, the first recurrences were highly

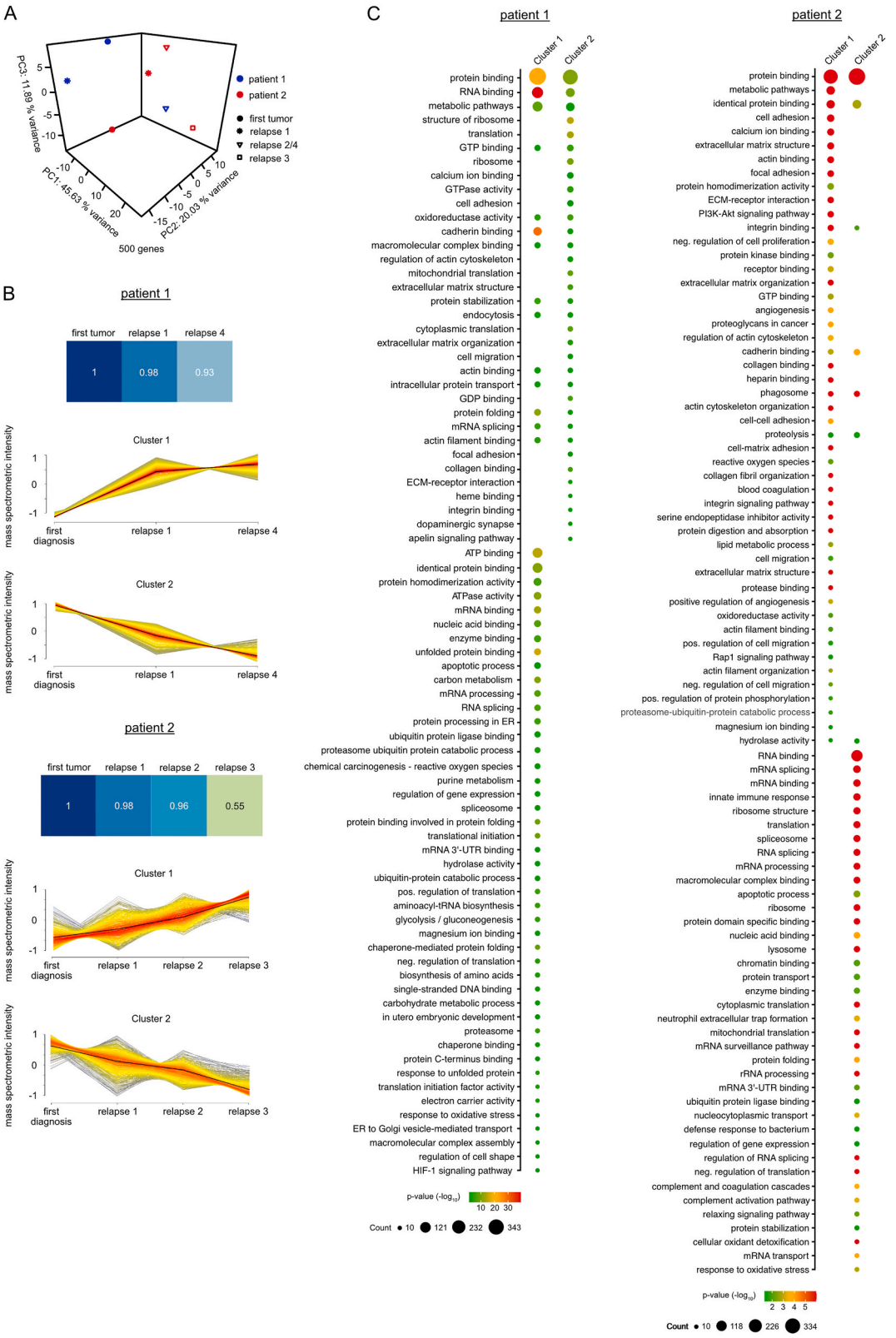

Fig. 5. A) A PCA of the longitudinal tumor samples of patient 1 and 2. B) A PCM compares the proteome of the first tumor to the relapses for each patient. Clusters are showing the dynamics and kinetics of protein production during disease progression. C) The DAVID-based analysis of each cluster predicts underlying molecular processes.

similar to the first tumor (98 %) (Fig. 5 B). Over time, the similarity decreased with each following recurrence, showing a considerable change in patient 2 with only 55 % identity between the first tumor and its third relapse (Fig. 5 B). Further, we used a clustering software to analyze the dynamics of protein production over time. For both patients, we detected proteins enriched (cluster 1) or depleted (cluster 2) during disease progression (Fig. 5 B). Additional clusters representing the different dynamics are given in Data S1 H. We identified the underlying molecular processes associated with the proteins found in each cluster by the DAVID algorithm (Fig. 5 C). In patient 1, proteins linked to cluster 1 (steadily increasing in intensity) can be associated with RNA and protein regulation and processing (mRNA/nucleic acid/enyzyme/protein binding, regulation of gene expression and translation), metabolic pathways, and embryonic development. Proteins linked to cluster 2 (steadily decreasing in intensity) can be associated with ECM interaction (e. g. ECM structure and organization, ECM-receptor interaction, cadherin/integrin/collagen binding), cell migration and adhesion (cell adhesion, focal adhesion). In patient 2, (in contrast to patient 1) proteins linked to cluster 1 can be associated with ECM interaction (e. g. ECM structure and organization, ECM-receptor interaction, cadherin/integrin/collagen binding and signaling), migration (regulation of migration, cell migration) and adhesion (cell adhesion, focal adhesion, cell-matrix adhesion). Proteins linked to cluster 2 can be associated with RNA and protein regulation and processing (e. g. mRNA/enzyme/protein binding, regulation of gene expression and translation).

4. Discussion

For metastatic GCT, GTS is a rare but serious condition having a poor prognosis. First described by Logothetis et al. [2], not much is known about GTS and its pathogenesis due to a small number of available cases so far. Treatment options are limited as GTS are resistant to chemo- and radiotherapy. Failure to detect GTS at early time points of manifestation leads to higher morbidity and mortality as GTS is growing quite fast and space demanding [3]. Thus, GTS patients harbor a higher risk to develop a STM [23,24]. This is the first study characterizing the clinical and molecular features of GTS on an (epi)genetic, transcriptional and proteome level. By this, we aimed at gaining insights into the underlying molecular pathogenesis of GTS and at identifying new biomarkers indicative for GTS.

Overall, patients diagnosed with GTS mainly present at primary metastatic stage with good prognosis and were treated with standard platin-based chemotherapy. However, GTS can also appear as metastatic recurrence or present with poor prognosis. Therefore, GTS seems to be unpredictable regarding clinical appearance, risk classification, received chemotherapy and tumor marker kinetics. Regarding the primary

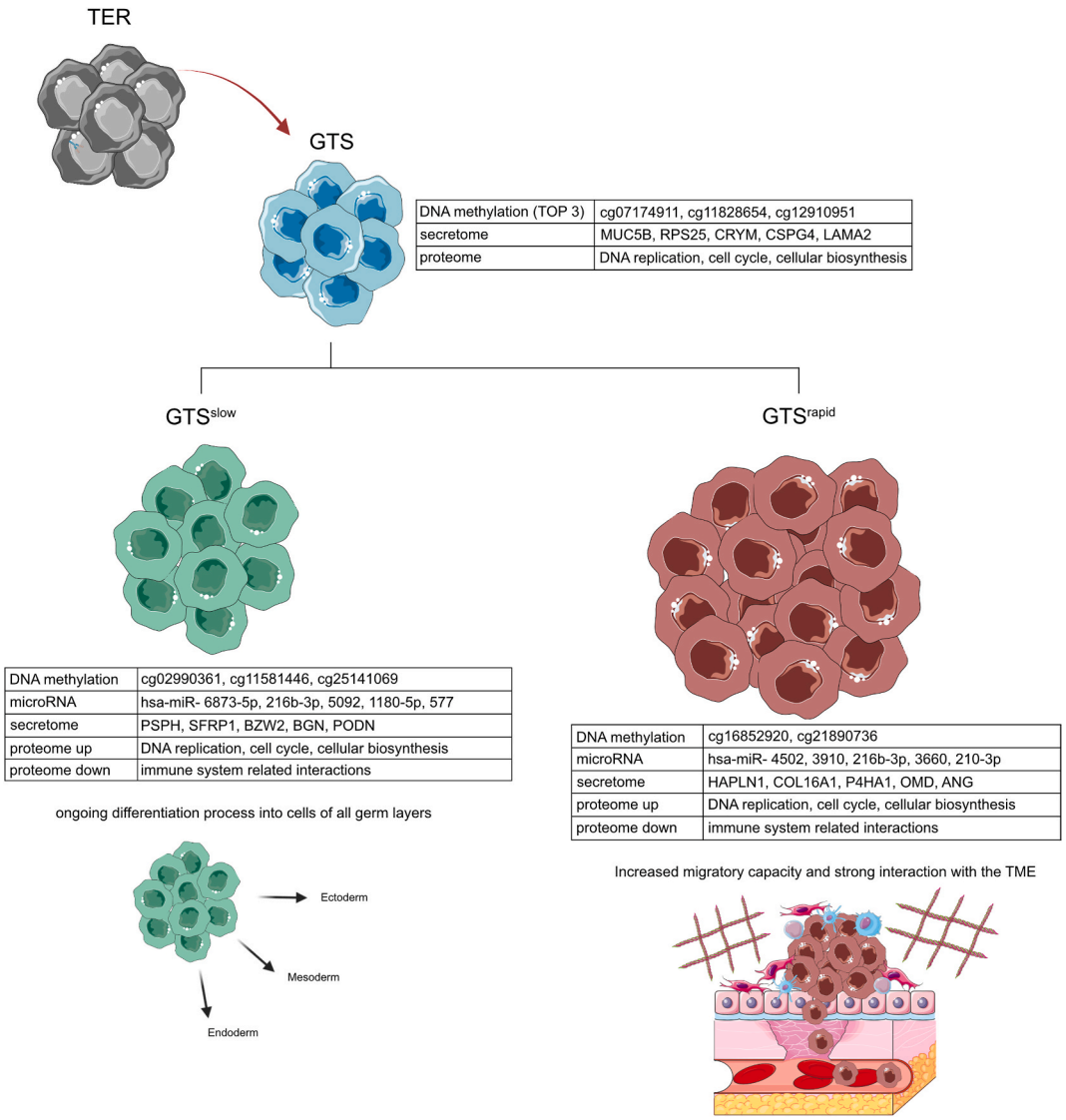

Fig. 6. Model summarizing molecular and epigenetic key findings of this study and highlighting most promising biomarkers.

orchiectomy histology, no pattern was found to predict the presence or development of GTS, as all histologic specimen contain teratomatous components (cells of all three germ layers). However, analyzing the distribution of the different histological GCT entities within our tumor growth classification, we found a higher proportion of YST in GTS^{rapid} (67 %) compared to GTS^{slow} (16 %) (Table 1), indicating YST as possible predictive component for a faster tumor progression.

On an epigenetic perspective, the overall DNA methylation landscape between the different GTS subgroups and TER were highly similar. Nevertheless, we could highlight individual hypermethylated CpG dinucleotides exclusively found in the different GTS subtypes (GTS^{slow} and GTS^{rapid}) as putative epigenetic biomarkers, as found in other tumor types [25–27] (Fig. 6). Additionally, we offer a set of microRNAs that might stratify between GTS$^{slow/rapid}$ and TER as well as GTS^{slow} and GTS^{rapid} (Fig. 6).

We extended our pool of possible circulating biomarkers by a LC-MS-based analysis of the secretome of GTS and TER. By this, we have deduced putative biomarkers for the different GTS groups or TER classified as 'secreted peptides' or 'unconventional protein secretion' (UPS) (Fig. 6). Especially UPS factors are of high interest and offer new opportunities for biomarker identification, since novel mechanism of protein shedding or secretion has been postulated for these factors normally detectable in the cytoplasm, leading to secretion of small peptide sequences from the full protein [28,29]. These putative biomarkers on epigenetic and secretome level might allow to detect GTS formation (at an early stage), and therefore rendering it possible to adjust the therapeutic concept in time to prevent further outgrowth of this space demanding tumor. Taken together, our study offers a set of secreted biomolecules as putative biomarkers for GTS/TER, setting the stage for future biomarker screenings.

Of note, Nestler et al. recently identified biomarkers (AGR2, KRT19) able to distinguish viable teratoma elements from necrosis [30]. We detected AGR2 in the proteome of TER and GTS patients, while KRT19 could be detected in the secretome only (Fig. S4 D; Data S1 D, F). Nevertheless, overall LC-MS intensities were quite low compared to the other putative biomarkers identified in this study and measurements did not reach the significance threshold (ANOVA p-value/q-value).

Furthermore, we analyzed GTS tissues on proteome and secretome level by LC-MS to identify molecular features of GTS. Consistent with its clinical behavior and continuous tumor growth compared to TER without a growth trend, proteins found enriched in GTS were involved in DNA replication and regulation, cell cycle and cellular biosynthetic processes (Fig. 6). Additionally, proteins interacting with the immune system and mediating pro-apoptotic processes were significantly depleted compared to TER, suggesting that GTS utilize mechanisms to escape the immune system and apoptotic processes, enabling an unimpeded tumor growth (Fig. 6).

From our 50 GTS patients, 8 suffered from teratoma recurrence, of which 3 developed a STM and 1 patient a considerable AFP elevation. In both longitudinal cases, we observed teratomatous recurrences and steadily increasing AFP levels over the time, resulting in formation of YST (both patients) and eventually even a STM (patient 1). Additionally, the majority of analyzed patients had a mixed GCT history at first diagnosis with increased serum markers AFP and beta-hCG (Table 1). Further, we detected expression of pluripotency and YST factors within the tested GTS samples, indicative of EC and/or YST subpopulations. These data support the idea of a residual, but pathological not detectable (occult) subpopulation of EC, YST or STM within the GTS. Although these occult elements might not be detectable in every patient, the definition by Logothetis et al. needs to be updated as it defines GTS as a pure and mature teratoma. We suggest the following definition:

The GTS describes a continuously growing teratoma that might harbor occult non-seminomatous components considerably reduced during therapy but outgrowing over time again.

Additionally, in the future our identified putative biomarkers, once validated to be suitable for detecting GTS in routine diagnostics, might be combined with detection of *microRNA371* or AFP to early detect regrowth of occult EC or YST elements, respectively [31–34].

We observed a considerably decreasing similarity in the proteome with each longitudinal recurrence in the GTS^{rapid} patient [2], showing a similarity of only 55 % to the first tumor after four years. In contrast, the recurrence of the GTS^{slow} patient [1] still showed a similarity of 93 % after nine years. Regarding the metastatic localization, GTS^{rapid} metastasized also into lung and brain, while GTS^{slow} relapsed only inside the retroperitoneum. These data suggest that patients of GTS^{rapid} subgroup do not only suffer from a faster tumor growth, but also from a more aggressive disease progression with the ability to migrate more easily into other parts of the body. The characterization of the molecular processes associated with the changes in the proteome in both longitudinal patients suggests that in the GTS^{slow} patient, the tumor is considerably altering its gene expression profile and that a differentiation process into the three germ layers is still ongoing, while a diminished interaction with the tumor microenvironment (TME) and migratory capacity could be observed over time, which is in line with an ongoing differentiation process and a limited tendency to metastasize. In contrast, in the GTS^{rapid} patient, a strongly enhanced interaction with TME including migration could be observed, putatively explaining its tendency to metastasize quickly.

In summary and translating our findings to the clinic, our study shed light on the poorly understood molecular and epigenetic features of GTS and we updated the definition of a GTS. We provide a repertoire of biomolecules that might serve as secreted biomarkers on molecular and epigenetic level for future pathological routine diagnostics. The GTS subgroup-specific biomarkers may offer valuable guidance to physicians in their decision-making, suggesting immediate surgical intervention in cases of GTS^{rapid}, while recommending active surveillance for GTS^{slow} as the more appropriate approach. By this, the quality of life for patients is improved by avoiding unnecessary treatments. Nevertheless, suitability of these biomarkers needs to be validated in future studies first. Additionally, our molecular analysis may help to identify GTS-specific therapeutic concepts, e. g. we identified cell cycle-associated and regulating proteins to be enriched in GTS samples, thus, testing cell cycle inhibitors might be a reasonable approach in future studies.

Ethics approval and consent to participate

The ethics committees of the Heinrich Heine University Düsseldorf and the University of Cologne raised no concerns on utilizing the tissue samples and corresponding clinical data for research (votes 2020-1247 and 21-1108, respectively).

Consent for publication

All authors are aware of this article and agreed on publication.

Availability of data and materials

All data generated or analyzed during this study are included in this published article and its supplementary information files or can be requested from the corresponding author. 850k DNA methylation array and microRNA sequencing data have been uploaded to Gene Expression Omnibus (GEO; https://www.ncbi.nlm.nih.gov/geo/) (GSE24009, GSE251975). LC-MS data generated in this study can be accessed via ProteomeXchange (http://www.proteomexchange.org) (PXD043529).

Funding

P. Pongratanakul was supported by the 'Junior Clinician Scientist' program of the 'Forschungskommission' of the Medical Faculty of the Heinrich Heine University, Düsseldorf. F. Bremmer was supported by the 'Wilhelm Sander-Stiftung' (2016.041.1/ .2/ .3). MicroRNAseq analysis were performed under support by the 'DFG Research

Infrastructure NGS_CC' (project 407495230) as part of the 'Next Generation Sequencing Competence Network' (project 423957469).

CRediT authorship contribution statement

Pailin Pongratanakul: Writing – review & editing, Writing – original draft, Visualization, Validation, Investigation, Funding acquisition, Formal analysis. **Felix Bremmer:** Resources, Investigation, Funding acquisition, Formal analysis, Conceptualization, Writing – review & editing. **Stella Pauls:** Software, Investigation, Formal analysis, Data curation. **Gereon Poschmann:** Software, Methodology, Investigation, Formal analysis, Data curation. **Catena Kresbach:** Investigation, Formal analysis. **Fatma Parmaksiz:** Investigation. **Margaretha A. Skowron:** Formal analysis, Visualization. **Janina Fuß:** Formal analysis, Investigation, Software. **Alexa Stephan:** Methodology, Investigation. **Pia Paffenholz:** Formal analysis. **Kai Stühler:** Resources, Methodology, Writing – review & editing. **Ulrich Schüller:** Resources, Methodology, Writing – review & editing. **Philipp Ströbel:** Resources, Writing – review & editing. **Axel Heidenreich:** Resources, Writing – review & editing. **Yue Che:** Writing – original draft, Investigation, Writing – review & editing. **Peter Albers:** Resources, Writing – review & editing. **Daniel Nettersheim:** Writing – review & editing, Writing – original draft, Visualization, Supervision, Resources, Project administration, Methodology, Formal analysis, Data curation, Conceptualization, Investigation.

Declaration of competing interest

The authors declare that they have no known competing financial interests or personal relationships that could have appeared to influence the work reported in this paper.

Acknowledgements

We kindly thank Anna Pehlke and Olga Dschun for excellent technical assistance.

We kindly thank Prof. Tilman Rau and Mara Walther (Institute for Pathology, UKD) for their support and access to the local biobank.

Appendix A. Supplementary data

Supplementary data to this article can be found online at https://doi.org/10.1016/j.canlet.2024.216673.

References

[1] L. Cheng, P. Albers, D.M. Berney, D.R. Feldman, G. Daugaard, T. Gilligan, et al., Testicular cancer, Nat. Rev. Dis. Prim. 4 (2018) 29.
[2] C.J. Logothetis, M.L. Samuels, A. Trindade, D.E. Johnson, The growing teratoma syndrome, Cancer 50 (1982) 1629–1635.
[3] P. Paffenholz, D. Pfister, V. Matveev, A. Heidenreich, Diagnosis and management of the growing teratoma syndrome: a single-center experience and review of the literature, Urol. Oncol.: Seminars and Original Investigations 36 (2018) 529.e23–529.e30.
[4] D.J. Lee, H. Djaladat, N.N. Tadros, M. Movassaghi, T. Tejura, V. Duddalwar, et al., Growing teratoma syndrome: clinical and radiographic characteristics, Int. J. Urol. 21 (2014) 905–908.
[5] M. Stella, A. Gandini, P. Meeus, I. Aleksic, A. Flechon, C. Cropet, et al., Retroperitoneal vascular surgery for the treatment of giant growing teratoma syndrome, Urology 79 (2012) 365–370.
[6] P.E. Spiess, W. Kassouf, G.A. Brown, A.M. Kamat, P. Liu, J.A. Gomez, et al., Surgical management of growing teratoma syndrome: the M. D. Anderson cancer center experience, J. Urol. 177 (2007) 1330–1334.
[7] F. Bremmer, H. Bohnenberger, S. Küffer, T. Oellerich, H. Serve, H. Urlaub, et al., Proteomic comparison of malignant human germ cell tumor cell lines, Dis. Markers 2019 (2019) 1–14.
[8] F. Bremmer, P. Pongratanakul, M. Skowron, Y. Che, A. Richter, S. Küffer, et al., Characterizing the mutational burden, DNA methylation landscape, and proteome of germ cell tumor-related somatic-type malignancies to identify the tissue-of-origin, mechanisms of therapy resistance, and druggable targets, Br. J. Cancer 129 (2023) 1580–1589.
[9] M.A. Skowron, M. Vermeulen, A. Winkelhausen, T.K. Becker, F. Bremmer, P. Petzsch, et al., CDK4/6 inhibition presents as a therapeutic option for paediatric and adult germ cell tumours and induces cell cycle arrest and apoptosis via canonical and non-canonical mechanisms, Br. J. Cancer 123 (2020) 378–391.
[10] M.D. Robinson, A. Oshlack, A scaling normalization method for differential expression analysis of RNA-seq data, Genome Biol. 11 (2010) R25.
[11] M.D. Robinson, D.J. McCarthy, G.K. Smyth, edgeR : a Bioconductor package for differential expression analysis of digital gene expression data, Bioinformatics 26 (2010) 139–140.
[12] K. Ikeda, T. Monden, T. Kanoh, M. Tsujie, H. Izawa, A. Haba, et al., Extraction and analysis of diagnostically useful proteins from formalin-fixed, paraffin-embedded tissue sections, J. Histochem. Cytochem. 46 (1998) 397–403.
[13] C.S. Hughes, S. Moggridge, T. Müller, P.H. Sorensen, G.B. Morin, J. Krijgsveld, Single-pot, solid-phase-enhanced sample preparation for proteomics experiments, Nat. Protoc. 14 (2019) 68–85.
[14] K. Brenig, L. Grube, M. Schwarzländer, K. Köhrer, K. Stühler, G. Poschmann, The proteomic landscape of cysteine oxidation that underpins retinoic acid-induced neuronal differentiation, J. Proteome Res. 19 (2020) 1923–1940.
[15] V. Demichev, C.B. Messner, S.I. Vernardis, K.S. Lilley, M. Ralser, Dia-Nn, Neural networks and interference correction enable deep proteome coverage in high throughput, Nat. Methods 17 (2020) 41–44.
[16] V.G. Tusher, R. Tibshirani, G. Chu, Significance analysis of microarrays applied to the ionizing radiation response, Proc. Natl. Acad. Sci. USA 98 (2001) 5116–5121.
[17] L. Zhao, G. Poschmann, D. Waldera-Lupa, N. Rafiee, M. Kollmann, K. Stühler, OutCyte: a novel tool for predicting unconventional protein secretion, Sci. Rep. 9 (2019) 19448.
[18] Gao J, Arman Aksoy B, Dogrusoz U, Dresdner G, Gross B, Onur Sumer S, et al. Integrative Analysis of Complex Cancer Genomics and Clinical Profiles Using the cBioPortal. [cited 2023 Dec 5]; Available from: http://www.adobe.com/products/illustrator.html.
[19] E. Cerami, J. Gao, U. Dogrusoz, B.E. Gross, S.O. Sumer, A. Aksoy, et al., The cBio Cancer Genomics Portal: an Open Platform for Exploring Multidimensional Cancer Genomics Data [Internet], CANCER DISCOVERY, 2012, 401. Available from: http://aacrjournals.org/cancerdiscovery/article-pdf/2/5/401/1817590/401.pdf.
[20] J. de Jong, L.H.J. Looijenga, Stem cell marker OCT3/4 in tumor biology and germ cell tumor diagnostics: history and future, Crit. Rev. Oncog. 12 (2006) 171–203.
[21] W. Wruck, F. Bremmer, M. Kotthoff, A. Fichtner, M.A. Skowron, S. Schönberger, et al., The pioneer and differentiation factor FOXA2 is a key driver of yolk-sac tumour formation and a new biomarker for paediatric and adult yolk-sac tumours, J. Cell Mol. Med. 25 (2021) 1394–1405.
[22] J. de Jong, H. Stoop, A. Gillis, R. van Gurp, G.-J. van de Geijn, M de Boer, et al., Differential expression of SOX17 and SOX2 in germ cells and stem cells has biological and clinical implications, J. Pathol. 215 (2008) 21–30.
[23] C.V. Comiter, A.S. Kibel, J.P. Richie, M.R. Nucci, A.A. Renshaw, Prognostic features of teratomas with malignant transformation: a clinicopathological study of 21 cases, J. Urol. 159 (1998) 859–863.
[24] R.J. Motzer, A. Amsterdam, V. Prieto, J. Sheinfeld, V.V.V.S. Murty, M. Mazumdar, et al., Teratoma with malignant transformation: diverse malignant histologies arising in men with germ cell tumors, J. Urol. 159 (1998) 133–138.
[25] A. Schröck, A. Leisse, L. de Vos, H. Gevensleben, F. Dröge, A. Franzen, et al., Free-circulating methylated DNA in blood for diagnosis, staging, prognosis, and monitoring of head and neck squamous cell carcinoma patients: an observational prospective cohort study, Clin. Chem. 63 (2017) 1288–1296.
[26] D. Dietrich, O. Hasinger, L.L. Bañez, L. Sun, G.J. van Leenders, T.M. Wheeler, et al., Development and clinical validation of a real-time PCR Assay for PITX2 DNA methylation to predict prostate-specific antigen recurrence in prostate cancer patients following radical prostatectomy, J. Mol. Diagn. 15 (2013) 270–279.
[27] B. Schmidt, V. Liebenberg, D. Dietrich, T. Schlegel, C. Kneip, A. Seegebarth, et al., SHOX2 DNA Methylation is a Biomarker for the diagnosis of lung cancer based on bronchial aspirates, BMC Cancer 10 (2010) 600.
[28] G. Poschmann, J. Bahr, J. Schrader, I. Stejerean-Todoran, I. Bogeski, K. Stühler, Secretomics—a key to a comprehensive picture of unconventional protein secretion, Front. Cell Dev. Biol. 10 (2022).
[29] L. Zhao, G. Poschmann, D. Waldera-Lupa, N. Rafiee, M. Kollmann, K. Stühler, OutCyte: a novel tool for predicting unconventional protein secretion, Sci. Rep. 9 (2019) 19448.
[30] T. Nestler, L. Kremer, M. von Brandenstein, M. Wittersheim, P. Paffenholz, S. Wagener-Ryczek, et al., Differentially expressed messenger RNA/proteins can distinguish teratoma from necrosis in postchemotherapy retroperitoneal lymph node dissection tissue, Cancer 129 (2023) 634–642.
[31] K.-P. Dieckmann, A. Radtke, L. Geczi, C. Matthies, P. Anheuser, U. Eckardt, et al., Serum levels of MicroRNA-371a-3p (M371 test) as a new biomarker of testicular germ cell tumors: results of a prospective multicentric study, J. Clin. Oncol. 37 (2019) 1412–1423.
[32] J.T. Lafin, N. Singla, S.L. Woldu, Y. Lotan, C.M. Lewis, K. Majmudar, et al., Serum MicroRNA-371a-3p levels predict viable germ cell tumor in chemotherapy-naïve patients undergoing retroperitoneal lymph node dissection, Eur. Urol. 77 (2020) 290–292.
[33] J. Piao, J.T. Lafin, C.G. Scarpini, M.M. Nuño, I. Syring, K.-P. Dieckmann, et al., A multi-institutional pooled analysis demonstrates that circulating miR-371a-3p alone is sufficient for testicular malignant germ cell tumor diagnosis, Clin. Genitourin. Cancer 19 (2021) 469–479.
[34] A.J.M. Gillis, M.A. Rijlaarsdam, R. Eini, L.C.J. Dorssers, K. Biermann, M.J. Murray, et al., Targeted serum miRNA (TSmiR) test for diagnosis and follow-up of (testicular) germ cell cancer patients: a proof of principle, Mol. Oncol. 7 (2013) 1083–1092.